Human Brain Tissue Identification Using Coherent Anti-Stokes Raman Scattering Spectroscopy and Diffuse Reflectance Spectroscopy for Deep Brain Stimulation Surgery

Sébastien Jerczyński
Université Laval
Mireille Quémener
Université Laval
Valérie Pineau Noël
Université Laval
Antoine Rousseau
Université Laval
Elahe Parham
Université Laval
Alexandre Bédard
Université Laval
Shadi Masoumi
Université Laval
Thomas Charland
Université Laval
Anthony Drouin
Université Laval
Jonathan Roussel
Université Laval
Valérie Dionne
Université Laval
Thomas Shooner
Université Laval
Anaïs Parrot
Université Laval
Mohamad Takech
Université Laval
Éric Philippe
Université Laval

Damon DePaoli
The Wellman Center for Photomedicine
Léo Cantin
Centre hospitalier de l'Université Laval
Martin Parent
Université Laval
Daniel Côté
dccote@cervo.ulaval.ca

Université Laval

Article

Keywords:

Posted Date: November 28th, 2023

DOI: https://doi.org/10.21203/rs.3.rs-3626764/v1

Additional Declarations: No competing interests reported.

Abstract

We assess the feasibility of using diffuse reflectance spectroscopy (DRS) and coherent anti-Stokes Raman scattering spectroscopy (CARS) as optical tools for human brain tissue identification during deep brain stimulation (DBS) electrode insertion, thereby providing a promising avenue for additional real-time neurosurgical guidance.

DRS and CARS spectra were acquired using a custom-built optical probe integrated in a commercial DBS lead. The electrode was inserted to target 3 specific regions in each of the brain hemispheres of a human cadaver, for a total of 6 insertions. DRS and CARS spectra were acquired during the lead insertion at constant position increments. Spectra were analyzed using a dimensionality-reduction technique, principal component analysis (PCA), and the *k-means* clustering method to classify each spectrum as being either white matter or gray matter for each trajectory. The results were compared to visual tissue classifications performed on histological brain sections and classifications based on a preoperative magnetic resonance imaging (MRI) scan.

DRS and CARS spectra obtained using the optical probe can identify white and gray matter during DBS lead insertion. In addition, the tissue composition along the trajectory toward a specific target is unique and can be differentiated by the optical probe. Moreover, the results obtained with PCA results suggest that DRS might be able to detect the presence of blood in front of the optical probe due to the strong optical absorption of hemoglobin in this wavelength range.

It is possible to use optical measurements from the DBS lead during surgery to identify white and gray matter, and possibly the presence of blood in human brain tissue. This information could provide better guidance in real time and prevent hemorrhages without disrupting the normal surgical workflow. Further developments are required to fully integrate these tools into standard clinical procedures.

Introduction

Parkinson's disease (PD) is the second most common neurodegenerative disorder after Alzheimer's disease[1]. The primary clinical signs of PD are motor symptoms that include resting tremors, muscular rigidity, and slowness of movements[2]. The initial treatment of PD usually starts by administering the dopamine precursor L-Dopa. However, over time, this pharmacological treatment becomes less effective and most patients will eventually suffer from L-Dopa-induced dyskinesia[3,4]. For these patients, deep brain stimulation (DBS) surgery is often the recommended treatment option[5].

DBS is widely recognized as the most effective surgical treatment for movement disorders, in particular, PD[6,7]. The surgery targets a specific brain region with an electrode that emits high-frequency electrical pulses[8], leading to a significant reduction in PD motor symptoms and improving quality of life. The target regions are deep subcortical nuclei that are typically components of the basal ganglia. According to the progression of the disease and hospital protocols, the optimal target region for PD is either the

subthalamic nucleus (STN) or the internal globus pallidus (GPi)[9]. Since those targets are only a few millimeters in size, a high level of expertise as well as precise navigation tools are needed for accurate DBS lead placement.

Current DBS procedures require three key steps before the surgery can begin: (1) localize the target region in the patient's brain, (2) determine the entry point, and (3) plan the trajectory to the target. Those steps are commonly performed preoperatively using magnetic resonance imaging (MRI) registered with stereotactic atlases[10]. In addition, microelectrode recordings (MERs) are often used to map the brain along the planned trajectory and confirm the target location prior to lead insertion[11–13]. However, this microelectrode is pulled out before the stimulation lead is inserted in the MER-identified target. Although this methodology is well established, the MER is only a proxy for the DBS lead. Many DBS surgeries therefore result in suboptimal lead placement for several reasons. First, the use of intraoperative MERs itself does not always provide better surgical outcomes[14,15]. For example, the presence of active neurons in white matter (WM) and electrically silent neurons in gray matter (GM) bias MER interpretations[14,16]. Second, MER is a time-consuming technique[17] that is not available at all health centers. Third, drilling a burr hole to open the skull can lead to cerebrospinal fluid leakage, possibly resulting in brain shifts greater than 2 mm[18–20], which is significant considering the small size of the DBS targets. The consequences of lead misplacements for patients are important: it might cause undesirable side effects such as paresthesia, oculomotor disturbances, affective changes, dysarthria and neuropsychological disorders such as depression that might require an additional surgery[15,21,22]. In 2000, a study demonstrated that approximately 45% of DBS surgeries resulted in DBS lead misplacements of over 3 millimeters from the originally intended target[23]. Another study showed that 41% of PD patients that complained about suboptimal surgery outcomes had a misplaced DBS lead[24]. Providing neurosurgical guidance from real-time *in situ* measurements could streamline the surgical process for both the surgical team and the patient, decrease the surgery time, reduce the overall treatment cost, and prevent adverse neuropsychological consequences.

Optical techniques are well suited to address the need for real-time feedback and have already shown potential for implementation in clinics[25,26].

Past studies from our research laboratory have introduced 2 fiber-based methods of choice for neurosurgical guidance: wavelength-swept coherent anti-Stokes Raman spectroscopy (CARS)[27] and diffuse reflectance spectroscopy (DRS)[28]. CARS is a label-free spectroscopy technique capable of probing unique molecular bonds. CARS is suitable for brain sensing and imaging due to the abundance of CH_2 bonds in myelinated axons. This abundance provides a strong and molecularly-specific contrast between WM and GM. Using a wavelength-swept source for CARS is more appropriate for highly-scattering, thick tissues compared to a spectrometer based measurement[29]. DRS takes advantage of low-cost broadband light sources to quantify the scattering and absorption properties of various brain structures (more details in [28]).

Here, we show the first use of these spectroscopic methods for brain-tissue identification in fresh human cadavers during DBS surgery. We performed the measurements inside a chronically-implanted DBS lead by replacing a commercial rigid stylet with another custom stylet, housing fiber optics. The enhanced lead was inserted to target the STN, the GPi, and one off-target region, in both hemispheres. The optical measurements were taken within a functional operating room, using our custom, mobile optical console. The tissue was identified using a spectral analysis dimensionality reduction technique called principal component analysis (PCA) with the *k-means* clustering method to classify each spectrum as either WM or GM for each point along the trajectory. To assess the viability of our collection of optical measurements, we used histological slices and MRI scans as references. Our findings suggest that optical measurements have the potential for real-time neuronavigation in human DBS surgeries. Altogether, this work provides a clinically relevant proof-of-concept approach to provide uninvasive, real-time feedback during DBS lead implantation.

Results

We were able to acquire optical spectra along 6 trajectories in a postmortem human brain. The tissues were identified as WM or GM to produce modality-specific barcodes, as presented in Fig. 4. The L-STN tract in the MRI and on the histological cuts are presented in Fig. 4A and B respectively. The comparison of all barcodes for each trajectory is presented in Fig. 4C. Tissue identification was performed for all the optical spectra along one trajectory using PCA and *k-means* clustering. On first approximation, we noted that the first principal component (PC1) for individual trajectories explained over 98% of the data variance between the spectra. This means that PC1 alone could be sufficient for constructing the optical barcode, and that most of the differences are encoded in intensity variations. We observed that the optical barcodes share more similarities with the histological barcodes than the MRI barcodes for all trajectories.

Discussion

This work demonstrates the first successful attempt at acquiring CARS and DRS spectra of brain tissue for human DBS surgery. The DRS and CARS spectra from the optical probe can adequately differentiate WM and GM, as presented in Fig. 4C. The optical measurements generally agree with the tissue classification from the HISTO barcodes for the same trajectory. However, small differences between the HISTO and optical barcodes remain. Due to the long postmortem delay and the lack of tissue fixation, the insertion of the optical probe may have caused brain compression and shifts. This may in turn lead to incorrect associations between tissue identification and the probe position, as well as mismatched reference and optical barcodes. In addition, some basal ganglia components such as the striatum, the GPi and the GPe, contain bundles of myelinated axons (WM) that travel through the GM. Therefore, these brain regions could be interpreted as mixed matter. Since our analysis clustered the data into 2 groups and did not consider mixed matter, both the histology and optical identification could have incorrectly labeled the mixed matter as WM or GM. Although the CARS and DRS barcodes for each trajectory have similarities, we did not expect them to be identical since the entry point on the surface of the brain is

different, as presented in Fig. 1B. Despite these shortcomings, comparing all 3 barcodes (STN, GPi and OFF) for one optical modality (either DRS or CARS) shows visible differences, suggesting that the tissue composition for a specific trajectory is unique and can be recognized by our optical probe.

The barcode correspondence between optical and MRI barcodes was poor. This is because the MRI images do not have the contrast and resolution required to identify tissue type with pixel intensity alone. The lack of contrast in the basal ganglia in Fig. 4A demonstrates that anatomical landmarks are essential to infer the location of small and uncontrasted regions, such as the STN. While MRI is an indispensable imaging tool for planning DBS surgery, identifying brain regions rely on the surgeon's knowledge of neuroanatomy.

Our experiment presents a proof-of-concept of optical measurements for tissue identification in the human brain, demonstrating its potential as a real-time DBS guidance tool for neurosurgeons. More measurements should be collected in clinical trials to assess the variability of the barcodes for specific targets. Our group is also investigating the use of other modalities, such as polarization-sensitive optical coherence tomography, as it measures the birefringence of the myelin[31]. We hypothesize that with more data and advanced analysis algorithms, optical barcodes could reflect MRI data. Our tool could provide real-time insights on lead insertion accuracy as the neurosurgeon performs the procedure.

The findings of this research indicate that DRS is a simple and minimally invasive optical method that could provide additional insight during DBS lead insertion. The PCA analysis revealed that the tissue identification is mostly accomplished by PC1 alone. The first 4 PCs from the L-OFF trajectory (DRS) are shown in Fig. 5A. PC1 for the L-OFF trajectory can be visualized as a straight line across all wavelengths, showing that the variance between the spectra acquired along the trajectory does not depend on the spectral information. This indicates that tissue identification is obtained only by the difference in light intensity that is scattered by the tissue. This observation is consistent with the inherent properties of brain tissue, where WM scatters more light than the darker GM tissue. It also suggests that measuring intensity of the light reflected at a single wavelength in the visible range, from the tissue in front of the DBS lead, could be sufficient to differentiate WM and GM using the analytical method we provided here.

Considering the wealth of information that is often encoded in an optical spectrum, looking at other PCs beyond PC1 might have the potential to improve tissue identification, as suggested in Fig. 5A. The absorption spectrum of blood (deoxyhemoglobin and oxyhemoglobin) is shown in Fig. 5B for comparison. The 2 peaks observed in PC4 approximately correspond to the 2 peaks found in the oxyhemoglobin absorption spectrum. The wider peak in PC3 is approximately at the same wavelength as the main peak found in the deoxyhemoglobin absorption spectrum. However, literature shows that oxyhemoglobin concentration decreases by 90% within 7h of death[32]. Therefore, it is not possible to conclude whether the optical probe detected very low concentrations of oxygenated blood or another unknown compound. Nevertheless, considering that oxyhemoglobin and deoxyhemoglobin are abundant in living subjects, it can be inferred that the spectroscopic measurements might reveal the presence of blood in the brain when inserting the optical probe. This could help prevent hemorrhaging and further

refine the tissue identification. However, since this experiment was conducted on a postmortem brain, it was not possible to confirm the plausibility of this hypothesis.

CARS showed promising results at tissue identification for PC1, which represents the intensity of the myelin signal in the tissue. However, attempts to use subsequent PCs for the analysis were unsuccessful despite using 10 mW of power and 8-second acquisitions at each depth along the trajectories. Indeed, only a very weak signal was detected and the signal-to-noise ratio was poor, revealing essentially no visible features in the spectral decomposition. Simple improvements could be made to our system to significantly enhance the CARS measurements quality. For example, since the laser wavelength is swept, the system could target specific vibrational modes that differentiate between WM and GM, such as 2845 cm^{-1} or 2880 cm^{-1}, which are abundant in myelin. This way, a spectrum would only have a handful of relevant points, which would increase the signal per wavelength with the same acquisition time by more than one order of magnitude. With this simple change, our probe could acquire a spectrum in under a second. Other technical improvements, such as optimizing the probe design for more efficient signal collection by adding collection fibers, could increase the signal-to-noise ratio.

For the first time, we have acquired CARS and DRS spectra in the brain of a human cadaver and have demonstrated how they can be used to identify tissue, offering a promising avenue for DBS surgical guidance. The spectra were acquired using a custom-built optical probe that was enclosed in a commercial DBS lead. The optical probe was then inserted, targeting 3 specific regions in the right and left hemispheres of the brain, for a total of 6 insertions. We observed that a barcode obtained from PCA and *k-means* clustering along a distinct trajectory appears unique. This demonstrates that the position of the lead could be followed in real time during its descent in the brain. In addition, DRS might be able to identify the presence of blood in the tissue to provide further guidance and prevent hemorrhages during lead insertion. More work is needed to refine the optical system to obtain higher quality spectral acquisitions and to design a probe that is suitable for trials in living patients. Finally, a rigorous strategy to map the optical barcode onto the preoperative MRI scans could provide the neurosurgeon with the much-needed real-time feedback.

Methods

Postmortem material was gathered from an 85-year-old man who died from metastatic prostate neoplasia, without any evidence of neurological, neurodegenerative or psychiatric diseases. The postmortem material was obtained from the Human Anatomy Laboratory at Université Laval and the brain was stored in the Human Brain Bank at CERVO Research Center. Both institutions required informed consent before tissue donation. Local ethics committees (*Institut universitaire en santé mentale de Québec*, 2013-3, 146–2012) approved collection procedures, storage, and handling of postmortem material. All methods were executed following relevant guidelines and regulations.

Twenty-four hours postmortem hours, the head was placed in phosphate-buffered saline (PBS). The surgery was performed 8 days later by a neurosurgeon at *Hôpital de l'Enfant-Jésus* (Québec, Canada),

who followed standard DBS protocol normally reserved for patients with PD. The brain tissue was not chemically preserved prior to the experiment.

Trajectory planning and preoperative MRI

Preoperative 3 Tesla MRI scans of the head were acquired (T1, T2 and FLAIR sequences) with a stereotactic frame (CRW, Radionics) that was used by the neurosurgeon to plan the lead insertion for 6 targets (STN, GPi and another off-target region in both hemispheres).

The StealthStation neuronavigation software was used to plan the 6 trajectories using a brain atlas, and to calculate the insertion angles, and determine the target coordinates. These parameters were then used for the lead insertions. The 2 angles (ring and arc) are shown in relation to the position of the head in Fig. 1A, and the values are listed in Table 1. The insertion trajectories can be visualized on the preoperative MRI scan on Fig. 1B. Note that, throughout the paper, we refer to the 6 trajectories by the hemisphere side (R: right, L: left) followed by the targeted region (STN, GPi and OFF for the off-target region).

Table 1
Insertion angles determined with the Medtronic StealthSation neuronavigation system for the six trajectories.

Target	R-STN	R-GPi	R-OFF	L-STN	L-GPi	L-OFF
Ring angle [°]	57.6	63.3	60.1	50.7	54.5	51.2
Arc angle [°]	-16.8	-12.7	-12.1	20.2	7.4	11.1

Surgery and spectroscopic measurements

A custom-built probe composed of 2 optical fibers for signal emission and one for signal collection was built by inserting the fibers into a stainless steel tube instead of the standard tungsten stylet (Fig. 2). This modified hollow-core stylet has similar rigidity to the original stylet. The probe was then inserted into a DBS lead (model 3389, Medtronic) with a cut-off tip to provide an exit-point for the fibers. The lead was then fixed to the micromanipulator, allowing optical measurements to be acquired along the insertion tract. More details on DRS and CARS methods can be found in the Supplementary Information.

A burr hole was drilled into the skull to access the brain. All spectral acquisitions began 40 mm before the target and continued for another 10 mm past the target, for a total length of 50 mm for each trajectory. CARS measurements were collected in the right hemisphere for a total of 3 trajectories (R-STN, the R-GPi and R-OFF), and DRS measurements were obtained using the same targets but in the left hemisphere (L-STN, L-GPi and L-OFF). Since CARS measurements had a long acquisition time (8 seconds), the insertion step size was set to 1 mm to minimize the overall duration of the surgery. For the DRS measurements, the acquisition time was short (500 ms) and therefore the insertion step size was reduced to 500 µm.

After completing the measurements, the probe was removed and a narrow glass capillary was inserted into the hole created by the probe using the exact same angles. This was done so the trajectories would be visible on the postoperative MRI.

Brain extraction and tissue manipulation

After the surgery, 13 days postmortem, the brain was extracted and fixed by immersing in 4% paraformaldehyde at 4°C for 2 days. The brain was then cut along the midline into the 2 hemispheres. For each hemisphere, coronal cuts were made along a 55° ring angle taken from the anterior-posterior commissure plane to provide a block of tissue containing the 6 trajectories. A third cut was made to separate the basal ganglia from the cerebral cortex. A schematic of the cuts and sections obtained is shown in Fig. 3. These blocks of tissue were fixed for 2 more days in 4% paraformaldehyde and then stored at 4°C in 0.1 M PBS containing 15% sucrose and 0.1% sodium azide. The blocks were sliced with a freezing microtome into 50 µm-thick transverse sections, which were serially collected and preserved at -20°C in an antifreeze solution composed of 30% glycerol and 30% ethylene glycol diluted in PBS. A top-view image of the block was recorded at each time a section was collected.

Tissue identification along the insertion tract via barcodes

Identification of the tissue type (WM, GM) at each point along the insertion tract produces what we called a *barcode*, which provides the specific spatial sequence of tissue along the path of the probe as approximated by the modality. One barcode was produced for each modality used in this study: MRI, histology, and optical spectroscopy. Despite having different spatial resolutions and contrasts, the MRI and histological barcodes (HISTO) were used as references for the optical barcodes. The following subsections explain how we extracted the barcodes for each modality and for each trajectory.

Visual tissue identification on histological brain slices

From the block of tissue containing the basal ganglia and the thalamus (block A in Fig. 3), sections in which lead tracts were visible were selected for further analysis. Different brain nuclei and brain regions were easily identified from the previously taken images using a brain atlas. As some brain regions are predominantly composed of WM or GM, identifying brain regions helped us determine the tissue type along the insertion tracts. When no specific brain structure could be clearly identified, the tissue type was classified based on the color of the tissue. Each section of the trajectory was classified as being either WM or GM. The results were then compiled to generate a unique barcode for each trajectory. This barcode serves as a ground truth for comparing the results of the spectral analysis.

Tissue identification using pre- and postoperative MRI scans

Tissue composition was determined from T1-weighted MRI scans by analyzing the pixel intensity levels in the preoperative images. On the postoperative scan, the insertion coordinates were identified on each transverse plane by examining the visible capillaries in the images. The preoperative scan was then

coregistered to the postoperative scan using the Advanced Normalization Tools (ANTs) software. Briefly, 2 linear transformations were applied, one for rigid transformation (rotation and translation) and another one for deformable transformation (shearing and scaling). Then, a non linear transformation was used (SyN), applying affine and deformable transformations based on cross-correlations on the image[30]. Tissue analysis was performed on the preoperative image according to the coordinates obtained from the registration. A pixel intensity threshold was selected to differentiate between WM and GM, and that determination was used to construct a barcode (see Supplementary Information).

Tissue identification using spectral analysis

A spectrum is a high-dimensional dataset where each level of intensity is considered an independent measurement. In trivial experiments (e.g., spectroscopy of clear liquids), a simple peak identification strategy is sufficient to unambiguously recognize a material. Here, that is not the case: there is no clear, obvious signature that can be easily observed. Therefore, CARS and DRS spectral data were analyzed using a dimensionality-reduction technique called Principal Components Analysis (PCA) and the *k-means* clustering technique to determine whether the probe was passing through WM or GM as it was inserted into the brain. PCA is a mathematical technique that reduces the complexity of a high-dimensional dataset. It identifies the most important patterns by finding a new set of variables, called principal components (PCs), which capture and quantify most of the variation in the original dataset. We applied PCA (with centering but without normalization) on the spectra for each individual tract. Then, the reduced dataset was used as an input in the *k-means* clustering technique to separate the data into *k* groups, of which there were 2 in our case. We interpreted the 2 groups as being WM and GM. From these results, 6 unique barcodes composed of either WM or GM were generated and compared to those obtained from the brain slices and MRI scans. More details about the spectral analysis methods are presented in the Supplementary Information.

Declarations

Data Availability

All the data obtained from this experiment is publicly available at https://www.dccmlab.ca/lab-documentation/.

Acknowledgments:

This work was supported by the Natural Sciences and Engineering Research Council (NSERC) Discovery Grant (RGPIN-2020-06936), the NSERC/HBI Chair in Optical Technologies for Neurosurgery (416330103) held by D.C. Côté, and the Canadian Institutes of Health Research grant (CIHR 114700) awarded to MP.

We would like to thank Patrick Desrosiers for his insightful advice on data analysis, Marc-Antoine Roy for his help with MRI scan registration, and Owen Ferguson and Delphine Breau for feedback on the manuscript.

Authors contributions

S.J., D.D., A.P., M.P., D.C.C, and L.C. planned and conducted the surgery. S.J., M.Q., and V.P.N. wrote the manuscript and took care of the modifications after review. S.J., M.Q., V.P.N., A.R., E.P., A.B., S.M., T.C., A.D., J.R., V.D. and T.S. contributed to the analysis. M.A.T. and E.P. extracted the head.

References

1. Poewe W, Seppi K, Tanner CM, et al. Parkinson disease. *Nature Reviews Disease Primers*. 2017;3(1):1–21.
2. Balestrino R, Schapira AHV. Parkinson disease. *Eur J Neurol*. 2020;27(1):27–42.
3. Armstrong MJ, Okun MS. Diagnosis and Treatment of Parkinson Disease: A Review. *JAMA*. 2020;323(6):548–560.
4. Rodriguez-Oroz MC, Obeso JA, Lang AE, et al. Bilateral deep brain stimulation in Parkinson's disease: a multicentre study with 4 years follow-up. *Brain*. 2005;128(Pt 10):2240–2249.
5. Ghika J, Villemure JG, Fankhauser H, Favre J, Assal G, Ghika-Schmid F. Efficiency and safety of bilateral contemporaneous pallidal stimulation (deep brain stimulation) in levodopa-responsive patients with Parkinson's disease with severe motor fluctuations: a 2-year follow-up review. *J Neurosurg*. 1998;89(5):713–718.
6. Perlmutter JS, Mink JW. Deep brain stimulation. *Annu Rev Neurosci*. 2006;29:229–257.
7. Miocinovic S, Somayajula S, Chitnis S, Vitek JL. History, applications, and mechanisms of deep brain stimulation. *JAMA Neurol*. 2013;70(2):163–171.
8. Breit S, Schulz JB, Benabid AL. Deep brain stimulation. *Cell Tissue Res*. 2004;318(1):275–288.
9. Butson CR, Maks CB, McIntyre CC. Sources and effects of electrode impedance during deep brain stimulation. *Clin Neurophysiol*. 2006;117(2):447–454.
10. Bjartmarz H, Rehncrona S. Comparison of accuracy and precision between frame-based and frameless stereotactic navigation for deep brain stimulation electrode implantation. *Stereotact Funct Neurosurg*. 2007;85(5):235–242.
11. Richter EO, Hoque T, Halliday W, Lozano AM, Saint-Cyr JA. Determining the position and size of the subthalamic nucleus based on magnetic resonance imaging results in patients with advanced Parkinson disease. *J Neurosurg*. 2004;100(3):541–546.
12. Au KLK, Wong JK, Tsuboi T, et al. Globus Pallidus Internus (GPi) Deep Brain Stimulation for Parkinson's Disease: Expert Review and Commentary. *Neurol Ther*. 2021;10(1):7–30.
13. Gross RE, Krack P, Rodriguez-Oroz MC, Rezai AR, Benabid AL. Electrophysiological mapping for the implantation of deep brain stimulators for Parkinson's disease and tremor. *Mov Disord*. 2006;21 Suppl 14:S259-S283.
14. Honey CR, Berk C, Palur RS, Schulzer M. Microelectrode recording for pallidotomy: mandatory, beneficial or dangerous? *Stereotact Funct Neurosurg*. 2001;77(1–4):98–100.

15. Bejjani BP, Damier P, Arnulf I, et al. Transient acute depression induced by high-frequency deep-brain stimulation. *N Engl J Med*. 1999;340(19):1476–1480.
16. Kiyatkin EA, Rebec GV. Striatal neuronal activity and responsiveness to dopamine and glutamate after selective blockade of D1 and D2 dopamine receptors in freely moving rats. *J Neurosci*. 1999;19(9):3594–3609.
17. McClelland S 3rd. A cost analysis of intraoperative microelectrode recording during subthalamic stimulation for Parkinson's disease. *Mov Disord*. 2011;26(8):1422–1427.
18. Pallavaram S, Dawant BM, Remple MS, et al. Effect of brain shift on the creation of functional atlases for deep brain stimulation surgery. *Int J Comput Assist Radiol Surg*. 2010;5(3):221–228.
19. Husch A, Hertel F. Chapter 6 - DBS imaging methods II: Electrode localization. In: Horn A, ed. *Connectomic Deep Brain Stimulation*. Academic Press; 2022:127–146.
20. Miyagi Y, Shima F, Sasaki T. Brain shift: an error factor during implantation of deep brain stimulation electrodes. *J Neurosurg*. 2007;107(5):989–997.
21. Krack P, Kumar R, Ardouin C, et al. Mirthful laughter induced by subthalamic nucleus stimulation. *Mov Disord*. 2001;16(5):867–875.
22. Berney A, Vingerhoets F, Perrin A, et al. Effect on mood of subthalamic DBS for Parkinson's disease: a consecutive series of 24 patients. *Neurology*. 2002;59(9):1427–1429.
23. Guridi J, Rodriguez-Oroz MC, Lozano AM, et al. Targeting the basal ganglia for deep brain stimulation in Parkinson's disease. *Neurology*. 2000;55(12 Suppl 6):S21-S28.
24. Okun MS, Tagliati M, Pourfar M, et al. Management of referred deep brain stimulation failures: a retrospective analysis from 2 movement disorders centers. *Arch Neurol*. 2005;62(8):1250–1255.
25. Jermyn M, Mok K, Mercier J, et al. Intraoperative brain cancer detection with Raman spectroscopy in humans. *Sci Transl Med*. 2015;7(274):274ra19.
26. Spliethoff JW, Prevoo W, Meier MAJ, et al. Real-time In Vivo Tissue Characterization with Diffuse Reflectance Spectroscopy during Transthoracic Lung Biopsy: A Clinical Feasibility Study. *Clin Cancer Res*. 2016;22(2):357–365.
27. DePaoli DT, Lapointe N, Messaddeq Y, Parent M, Côté D. Intact primate brain tissue identification using a completely fibered coherent Raman spectroscopy system. *Neurophotonics*. 2018;5(3):035005.
28. DePaoli D, Goetz L, Gagnon D, et al. Intraoperative fiber optic guidance during chronic electrode implantation in deep brain stimulation neurosurgery: proof of concept in primates. *J Neurosurg*. 2019;4:1–10.
29. Bégin S, Burgoyne B, Mercier V, Villeneuve A, Vallée R, Côté D. Coherent anti-Stokes Raman scattering hyperspectral tissue imaging with a wavelength-swept system. *Biomed Opt Express*. 2011;2(5):1296–1306.
30. Avants BB, Epstein CL, Grossman M, Gee JC. Symmetric diffeomorphic image registration with cross-correlation: evaluating automated labeling of elderly and neurodegenerative brain. *Med Image Anal*.

2008;12(1):26–41.

31. DePaoli D, Côté DC, Bouma BE, Villiger M. Endoscopic imaging of white matter fiber tracts using polarization-sensitive optical coherence tomography. *Neuroimage*. 2022;264:119755.
32. Gatto R, Hoffman W, Mueller M, Flores A, Valyi-Nagy T, Charbel FT. Frequency domain near-infrared spectroscopy technique in the assessment of brain oxygenation: a validation study in live subjects and cadavers. *J Neurosci Methods*. 2006;157(2):274–277.
33. Prahl S. Optical Absorption of Hemoglobin. https://omlc.org/spectra/hemoglobin/

Figures

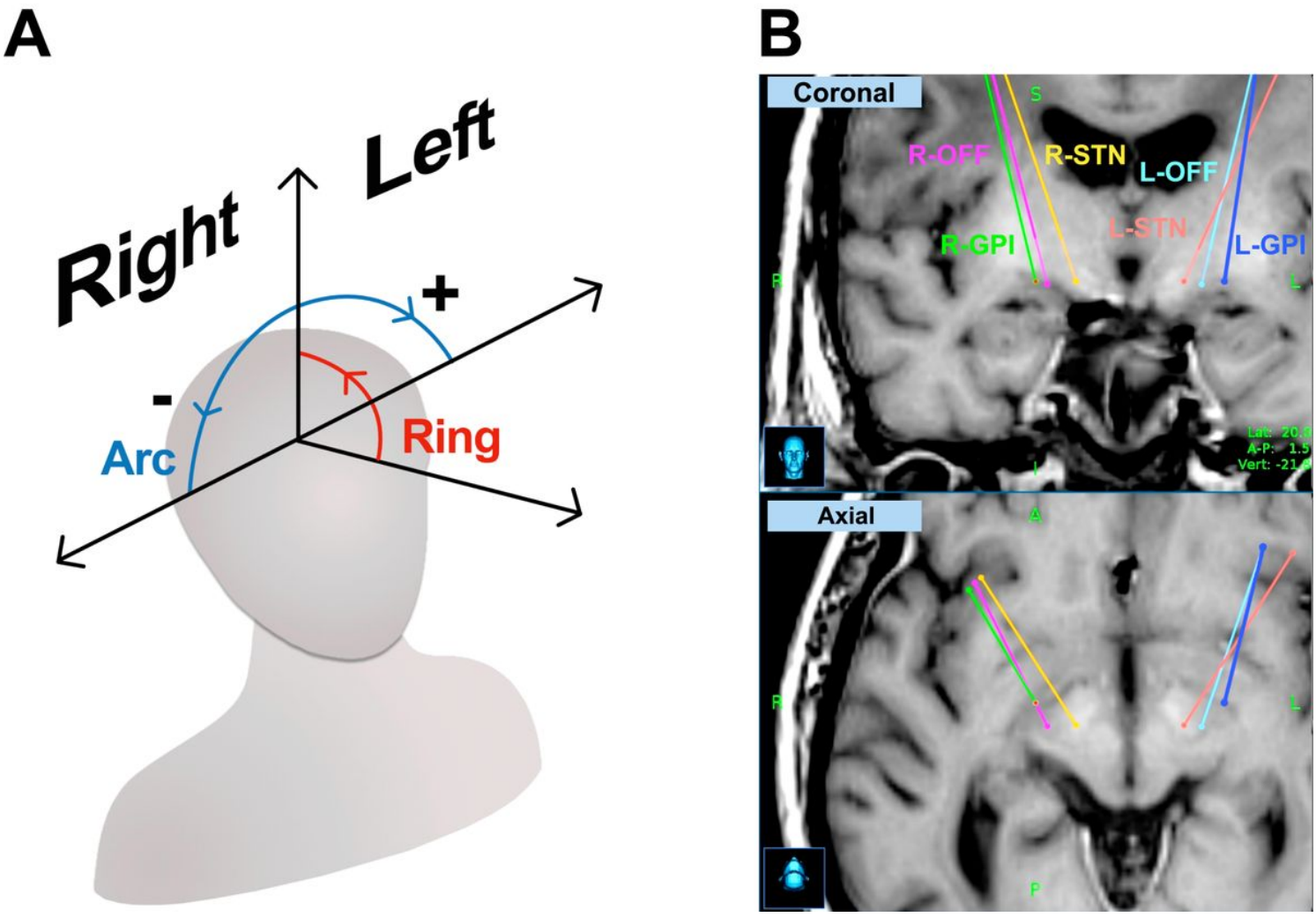

Figure 1

Trajectory planning prior to the DBS surgery. A: Coordinate system used for the insertion planning. The arc angle is positive for the left hemisphere and negative for the right hemisphere. B: Insertion angles determined with the Medtronic StealthSation neuronavigation system using the preoperative MRI scans for the 6 trajectories.

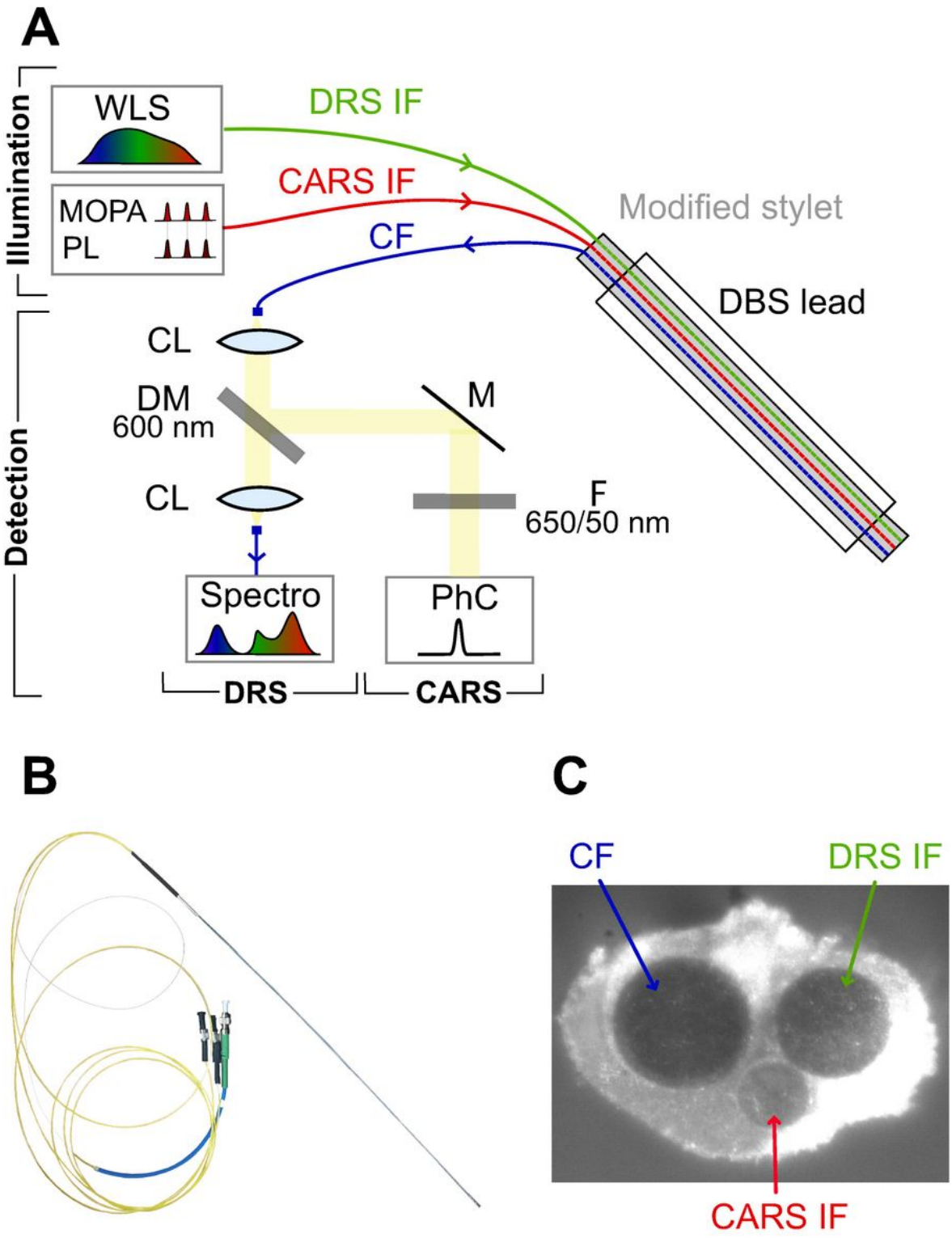

Figure 2

Optical probe and setup for illumination and collection for both CARS and DRS. A: Schematic diagrams of the probe and the acquisition setup. B: Photography of the optical probe composed of a Medtronic 3389 DBS lead containing a modified stylet (metallic tube) and 3 optical fibers enclosed. C: Photograph of the tip of the probe with the illumination and collection fibers visible. IF = illumination fiber; CF = collection fiber; CL = collimation lens; M = mirror; F = filter; WLS = white light source; MOPA = master

oscillator amplifier; PL = programmable laser; Spectro = spectrometer; PhC = photon counter. For the left hemisphere acquisitions without CARS, the CF was connected directly into the spectrometer to bypass the DM.

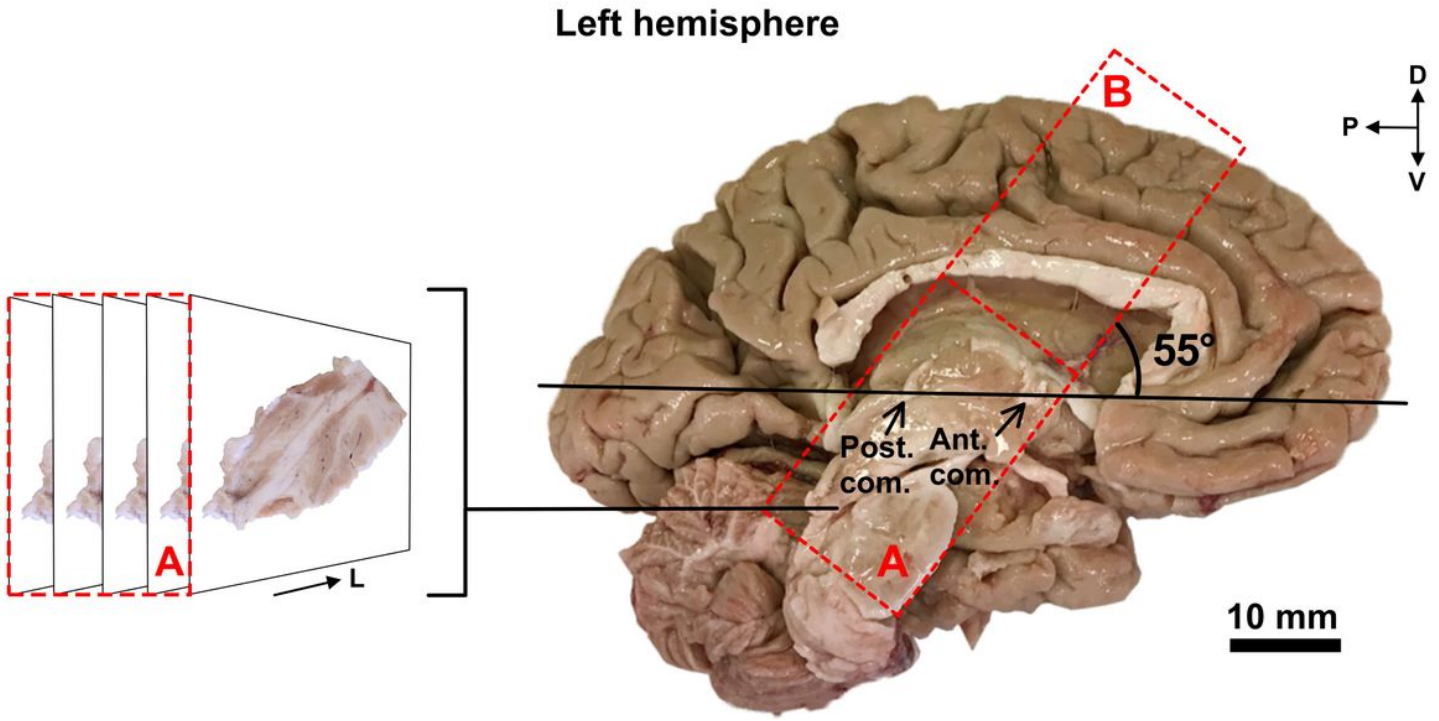

Figure 3

Dissection of the left hemisphere of the brain. In each hemisphere, the region of interest was cut into 2 blocks of tissue (A and B, defined by red dashed lines). The cuts were made at a 55° ring angle from the anterior-posterior commissure plane (shown in black) corresponding approximately to the ring angle used for the 6 trajectories. Each block was then fixed for 2 more days in paraformaldehyde and cut into 50 µm-thick sections using a freezing microtome. While cutting, a picture of each histological section was taken. Only the images from block A were used for analysis. D = dorsal; V = ventral; P = posterior; L = lateral.

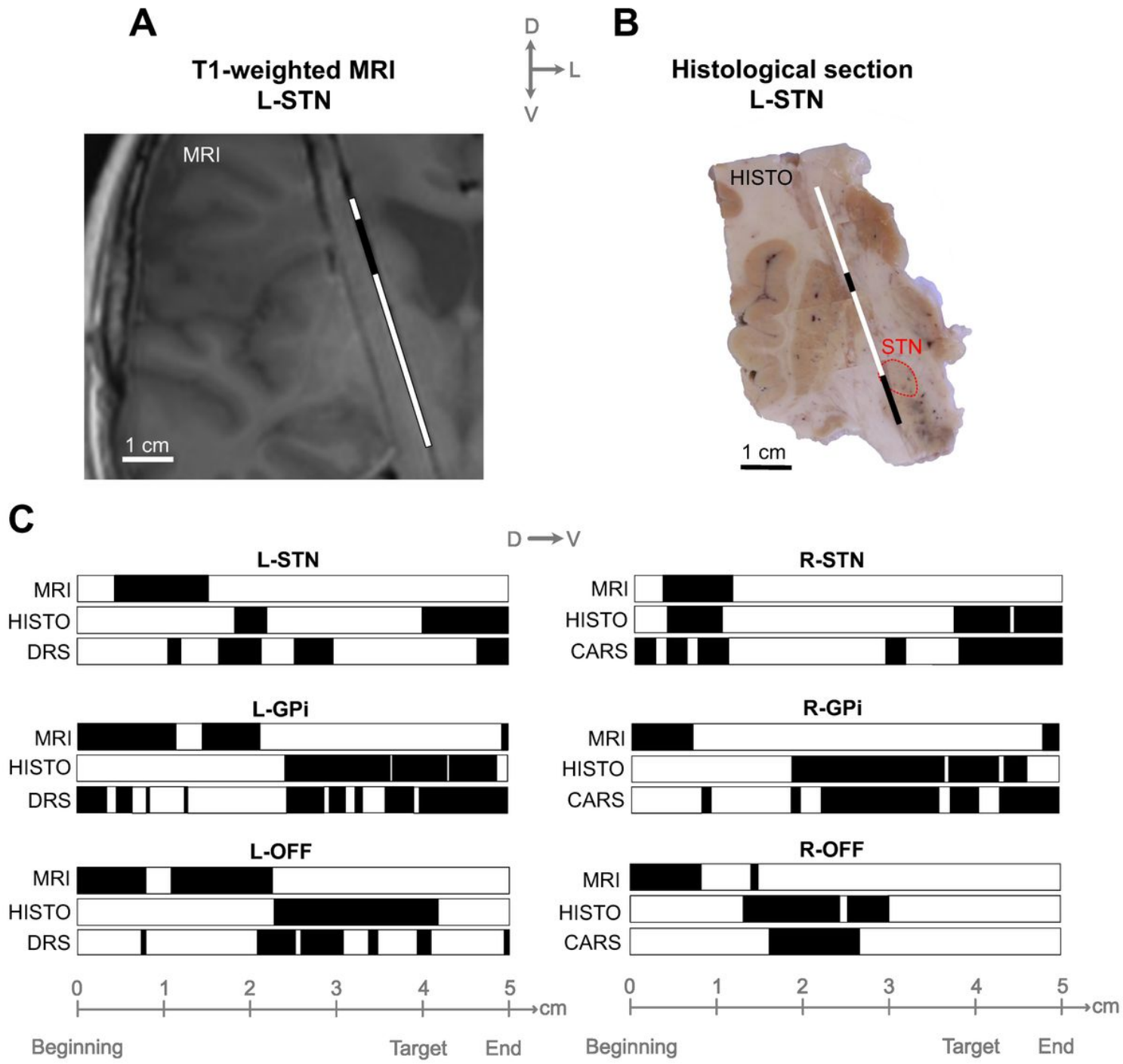

Figure 4

A: Example of an MRI plane showing the insertion trajectory for L-STN and the corresponding barcode. B: Example of barcode generation on a histological section where the trajectory for L-STN is visible. D = dorsal; L = lateral; V = ventral. C: Barcodes from MRI, histology (HISTO), and from spectral acquisitions (CARS or DRS) using spectral analysis (PCA) and the clustering algorithm *k-means* to classify the tissue as white matter (WM; white bars) or gray matter (GM; black bars) for each spectrum along the 6 insertion trajectories.

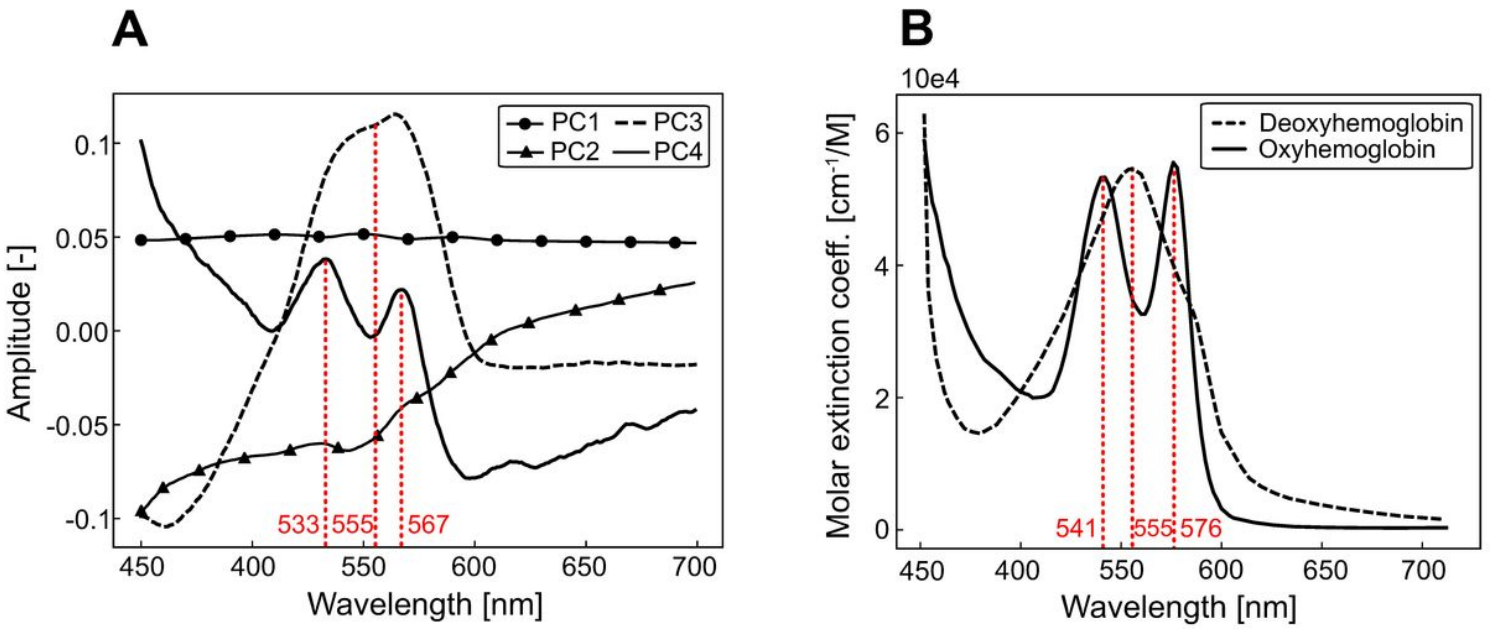

Figure 5

A: The 4 first principal components obtained with the PCA algorithm for the L-OFF trajectory. For the L-OFF trajectory, PC1 explained 98.937% of the variance of the spectral dataset, and PC2, PC3, and PC4 explained approximately 0.09%, 0.01%, and 0.002% respectively. B: Deoxyhemoglobin and oxyhemoglobin absorption spectra obtained from [33]. PC3 and PC4 show similarities to the absorbance peaks for deoxyhemoglobin and oxyhemoglobin. These peaks in the spectrum are highlighted by the red, vertical dotted lines.

Supplementary Files

This is a list of supplementary files associated with this preprint. Click to download.

- figureS1.pdf
- figureS2.pdf
- SupplementaryInformation.docx